Catalytic Cracking of Alkanes on FAU: Single-Event Microkinetic Modeling Including Acidity Descriptors

Rhona Van Borm, Marie-Françoise Reyniers, and Guy B. Marin
Chemical Engineering Dept., Laboratory for Chemical Technology, Ghent University, Ghent 9000, Belgium

DOI 10.1002/aic.13831
Published online May 22, 2012 in Wiley Online Library (wileyonlinelibrary.com).

Single-event microkinetic (SEMK) modeling is applied to catalytic cracking of 2,2,4-trimethylpentane on a series of faujasites with Si/Al ratio ranging from 2.6 to 30. Standard activation entropies of the various elementary reaction families are calculated a priori *from transition state theory and statistical thermodynamics, while activation energies are estimated on a reference faujasite by regression to experimental kinetic data. The SEMK model is then extended with two acidity descriptors. The concentration of active sites is available from independent NH_3-TPD measurements, while the change in standard protonation enthalpy, relative to the reference faujasite, is obtained by regression to experimental kinetic data. The latter parameter accounts for the effect of the zeolite average acid strength both on the stability of the intermediates and on the activation energies of the protonation and protolytic scission reactions. For these five commercially available faujasites, a variation in standard protonation enthalpy of 29 kJ mol^{-1} was found.* © 2012 American Institute of Chemical Engineers *AIChE J,* 58: 2202–2215, 2012

Keywords: catalytic cracking, FAU, 2,2,4-trimethylpentane, acidity, SEMK, catalyst descriptors

Introduction

Catalytic cracking of hydrocarbons over a solid acid catalyst is one of the most important processes in today's oil refining industry.[1,2] Heavy oil fractions, such as vacuum gas oil and residues, are converted into lighter and more valuable oil fractions, typically gasoline, middle distillates, and light alkenes. An industrial FCC catalyst contains Y-type zeolite or faujasite as main active component. The worldwide consumption of FCC catalysts amounts to approximately 500 kt per year, making fluid catalytic cracking the largest consumer of zeolite catalysts.[1,3] The process is very flexible with respect to the process configuration, the feedstocks to be processed, and the catalyst, allowing the refiner to adjust the product yields to meet the market demands and environmental legislation.[2]

Faujasites used in industrial FCC catalysts are commonly dealuminated via thermal, hydrothermal, or chemical treatments to improve the thermal stability, physicochemical properties, and activity of the catalyst.[4,5] This treatment modifies the zeolite acid properties as well as its framework structure. During dealumination, Al atoms are removed from the zeolite framework resulting in a variety of extra-framework Al (EFAl) species, which are believed to be, at least partly, Lewis acid sites. At the same time, part of the framework is destroyed and mesopores are created. According to the next-nearest-neighbor (NNN) concept, the strength of the Brønsted acid sites depends on the number of NNN Al atoms.[6] For faujasites, the lowest strength corresponds to 9 NNN Al atoms or a Si/Al ratio of 1, whereas the highest strength corresponds to isolated Al atoms (0 NNN) or a Si/Al ratio higher than 11.[7] However, the effect of dealumination on the catalytic behavior of the zeolite is more complex due to the presence of EFAl. Several theories have been postulated in the literature concerning the influence of EFAl. It has been proposed that these EFAL species provide a more favorable reaction pathway to initiate the cracking cycle or that they interact with the Brønsted acid sites creating sites with higher strength and thus higher activity.[4,8,9]

In the literature, protolytic scission of alkanes on zeolites has been proposed as a suitable model reaction to evaluate the effect of the strength of the Brønsted acid sites on the catalytic activity.[9–12] This monomolecular reaction is of first order and involves proton transfer from the zeolite to the physisorbed hydrocarbon. The intrinsic activation energy of this reaction should thus be a measure for the acid strength of the zeolite. Assuming that the physisorption step is in equilibrium, Eq. 1 expresses the relationship between the observed cracking rate, the intrinsic protolytic scission rate, and the physisorption enthalpy and entropy. This leads to Eqs. 2 and 3 for the apparent activation energy and the apparent pre-exponential factor, respectively. Which of these factors are responsible for the observed activity and selectivity differences on monomolecular cracking of alkanes on zeolites with varying acid strength or framework type is still debated.

$$r = kK_{\text{phys}}p_i = \left[A\exp\left(-\frac{E_a}{RT}\right)\right]\left[\exp\left(\frac{\Delta S^0_{\text{phys}}}{R}\right)\exp\left(-\frac{\Delta H^0_{\text{phys}}}{RT}\right)\right]p_i \qquad (1)$$

Additional Supporting Information may be found in the online version of this article.

Correspondence concerning this article should be addressed to M.-F. Reyniers at mariefrancoise.reyniers@ugent.be.

$$E_{app} = E_a + \Delta H^0_{phys} \quad (2)$$

$$A_{app} = A \exp\left(\frac{\Delta S^0_{phys}}{R}\right) \quad (3)$$

Studies on monomolecular cracking of various *n*-alkanes on zeolites differing in framework type, Si/Al ratio, and amount of EFAl species indicate that the observed differences in catalytic activity are controlled by differences in physisorption enthalpies rather than by differences in acid strength.[9–12] A similar intrinsic activation energy for protolytic scission was found on all zeolites. However, in a recent study on monomolecular cracking of *n*-hexane and *n*-octane on a wide variety of zeolites, Katada et al.[13] found that the heat of physisorption could not be related to the cracking activity on each zeolite, indicating that rather the acid strength controls the cracking activity. Kotrel et al.[14] did not find a constant intrinsic activation energy either for protolytic scission of *n*-hexane on ZSM-5, BEA, or (US)Y zeolites, after taking the heat of physisorption into account. Bhan et al.[15] stated that, at typical reaction conditions for monomolecular cracking, differences in physisorption equilibrium coefficients K_{phys} cannot account for the observed differences in activity among different zeolite framework types because of the compensation effect between ΔH^0_{phys} and ΔS^0_{phys}. Differences in activity were attributed to differences in intrinsic pre-exponential factors as well as differences in intrinsic activation energies. De Moor et al.[16] also came to the conclusion that changes in monomolecular cracking activity with carbon number and with zeolite framework cannot be attributed solely to changes in the physisorption equilibrium coefficient, indicating that the intrinsic pre-exponential factors, and thus the intrinsic activation entropies, play an important role. Gounder and Iglesia[17,18] found that also the location of the Brønsted acid sites in a particular framework type influences the observed activity in monomolecular alkane cracking. This is explained by the dominant role of entropy in the stabilization of adsorbed species and transition states within confined spaces, where entropic gains can compensate for enthalpic penalties, resulting in a lower free energy for the transition state.

Kinetic models that explicitly account for the effect of acidity on the catalytic behavior are relatively scarce in the literature. Ramôa Ribeiro and coworkers have applied Brønsted–Evans–Polanyi type equations to derive activity–acidity relationships in ZSM-5 and (US)Y zeolites for catalytic cracking of various alkanes and for light olefin transformation.[19–25] These authors performed TPD using a strong base, ammonia or pyridine, to characterize the acid strength distribution of the zeolite and related the desorption activation energy to the global catalytic activity of the zeolite or to the rate coefficients of the reactions under study. This modeling technique thus introduces two model parameters per rate coefficient to account for the influence of acidity that are to be obtained via estimation. In their kinetic models, Dumesic and coworkers[26–29] have incorporated a single adjustable parameter, reflecting the heat of stabilization of a carbenium ion relative to the heat of stabilization of a proton by the zeolite, to describe the effect of acid strength on the cracking of isobutane and 2-methylpentane on a series of USY zeolites. This approach has also been applied by Klein and coworkers[30–32] to describe the cracking of various hydrocarbons on FAU and MFI zeolites. In our research group, so-called single-event microkinetic (SEMK) models that account explicitly for the influence of the acid strength on the reaction rates have been developed for hydroconversion of alkanes on Pt/USY zeolites.[33,34] A single catalyst dependent adjustable parameter, that is, a catalyst descriptor, that reflects the difference in standard protonation enthalpy between two catalysts, is introduced to account for the effect of the average acid strength on the composite activation energies, that is, the sum of the protonation enthalpy and the intrinsic activation energy of a surface reaction.

The aim of this work is to develop a fundamental modeling strategy, based on the SEMK modeling approach, which can describe the effect of acidity when cracking alkanes on a series of faujasites in the absence of coke formation. In all the SEMK models for catalytic cracking that have been developed previously,[35–37] the single-event rate coefficients are still characteristic for a given catalyst. To improve the flexibility of the SEMK model and to reduce both the experimental and the parameter estimation effort, the SEMK model is extended to include catalyst descriptors that account explicitly for the effect of the catalyst acid properties on the observed activity and selectivity. In a previous study, catalytic cracking experiments were performed over a series of five commercially available faujasites with Si/Al_{bulk} ratio ranging from 2.6 to 30 using 2,2,4-trimethylpentane.[38] These kinetic data will be used in this study to determine kinetic descriptors, that describe the cracking of alkanes on a reference FAU, and catalyst descriptors, that describe the influence of the acid properties on the observed catalytic behavior. Pre-exponential factors are calculated, based on transition state theory and statistical thermodynamics, to decrease the number of kinetic descriptors to be estimated. First, kinetic descriptors are estimated by regression to the experimental data obtained on the reference catalyst LZ-Y20 ($Si/Al_{bulk} = 2.6$). Next, the SEMK model is extended to include a limited number of acidity descriptors, which allows to transpose the kinetic model to another zeolite with FAU framework. These acidity descriptors are estimated by regression to the experimental data obtained on the other faujasites. All experimental data were extrapolated toward time on stream zero to exclude the effect of coke formation, which is not taken into account. Catalytic cracking is thus modeled in the absence of coke formation and the effect of acidity thus relates to the fresh zeolite. In this work, a detailed molecular level kinetic model is used instead of the relumped models used previously, which included predefining certain sequences of elementary reaction steps into a global reaction.[35–39] The main advantage of such molecular level model is that all carbenium ion intermediates are explicitly accounted for and no *a priori* reaction pathways are assumed. Therefore, the effect of acidity can be evaluated on each elementary reaction step individually instead of evaluating this effect on a global reaction pathway only. Hence, this way a more fundamental understanding of the effect of acidity on reaction kinetics is obtained.

Experimental

Catalysts

Catalytic cracking data obtained on a series of five commercially available faujasites differing in acid properties are used to develop the kinetic model. Three USY zeolites were purchased from Zeolyst International. Steaming of a parent zeolite with Si/Al ratio of 2.6 produces CBV500, while a second steam treatment at higher temperature, followed by

Table 1. Reaction Network Taken into Account to Estimate SEMK Rate Coefficients for Acyclics Cracking

Hydrocarbon Species	Elementary Reaction Steps
35 alkanes	179 protolytic scissions
	78 hydride transfers
94 alkenes	137 protonations
102 alkylcarbenium ions	88 hydride shifts
	36 methyl shifts
	193 PCP-isomerizations
	21 β-scissions
	6 alkylations
	161 deprotonations

acid leaching, results in CBV720 and CBV760. Another USY (LZ-Y20) and one Y zeolite (Y62) were obtained from Union Carbide Corporation (currently UOP). The Si/Al_{bulk} ratio of these five zeolites ranges from 2.6 to 30. A detailed characterization of these faujasites is given elsewhere.[40–46] Table 1, Supporting Information summarizes the bulk and framework Si/Al ratio, the total molar concentration of acid sites, C_t, the BET surface area, S_{BET}, and the micropore volume, V_{micro}. The concentration of acid sites was determined via NH_3-TPD, as described by Niwa et al.[47]

Feedstocks and operating conditions

In a previous study,[38] 2,2,4-trimethylpentane was cracked on the five faujasites in Table 1, Supporting Information. 2,2,4-Trimethylpentane was selected as model molecule to represent alkane cracking. As a result of its high degree of branching, it cracks relatively fast, and it is the smallest molecule that can undergo all types of elementary reactions in the SEMK model describing alkane cracking. The conversion of 2,2,4-trimethylpentane is expressed as the number of moles of reactant converted per mole of reactant fed, while the selectivity toward product i is obtained as the number of moles of product i formed per mole of 2,2,4-trimethylpentane converted.

The operating conditions were chosen such that interference of thermal cracking was avoided and that monomolecular as well as bimolecular reactions occur. Temperature ranged from 698 to 763 K, reactant partial pressure was varied between 3 and 15 kPa, and space times between 8 and 215 kg_{cat} s mol^{-1} were applied thus covering a broad range of operating conditions including a conversion between 1 and 60 mol %. Table 2, Supporting Information summarizes the operating conditions, conversion range, and number of experiments performed on each catalyst.

Procedures and data processing

Parameter Estimation. Parameter estimates are obtained by minimizing the objective function $S(\boldsymbol{b})$ with respect to the model parameter vector $\boldsymbol{b}(b_j, j = 1,\ldots,p)$, which is assumed to approach the real parameter vector β when the optimum is reached. This objective function equals the weighted sum of the squared differences between the observed and the calculated molar outlet flow rates

$$S(\boldsymbol{b}) = \sum_{i=1}^{n}\sum_{j=1}^{v} w_j\left(F_{ij} - \hat{F}_{ij}\right)^2 \xrightarrow{\boldsymbol{b}} \text{minimum} \tag{4}$$

in which w_j are the weighting factors; F_{ij} and $\hat{F}_{ij}$ are the observed and the calculated molar outlet flow rates of species j in experiment i, respectively; n is the number of observations; and v is the number of responses per observation. The minimization of the objective function is performed by ODRPACK using a multiresponse Levenberg–Marquardt algorithm.[48] The nonlinear ordinary least squares option is used to estimate the parameters.

Assuming the experimental errors are uncorrelated, the weighting factors w_j correspond to the diagonal elements of the inverse error covariance matrix and can be calculated via Eq. 5

$$w_j = \frac{1}{\sigma_{jj}^2} = \frac{(nv - p)/v}{\sum_{i=1}^{n}\left(F_{ij} - \hat{F}_{ij}\right)^2} \tag{5}$$

First, simulations are performed to explore the parameter phase space and to obtain preliminary parameter estimates that were then used as starting values in the final parameter estimation procedure. In total, the responses of 129 gas-phase hydrocarbons are taken into account in the objective function (Eq. 4). Those that have been observed in the experiments with a product selectivity higher than 1 mol % are taken into account via Eq. 5. For hydrocarbons in the reaction network that were observed in lower quantities or not at all a weight factor equal to one was chosen. This way, relatively unimportant or unobserved responses are neither neglected during the parameter estimation nor assigned too much importance.

During the parameter estimation, a reparameterization is applied to the Arrhenius equation to center the data around the mean temperature, T_m, rather than T_∞. This leads to Eqs. 6 and 7 for any single-event rate coefficient, $\tilde{k}$, and the corresponding reparameterized pre-exponential factor, A_{rep}, respectively.

$$\tilde{k} = A_{rep}\exp\left[-\frac{E_a}{R}\left(\frac{1}{T} - \frac{1}{T_m}\right)\right] \tag{6}$$

$$A_{rep} = \tilde{A}\exp\left[-\frac{E_a}{RT_m}\right] \tag{7}$$

Note that, indeed, $A_{rep} = \tilde{k}(T_m)$, while $\tilde{A} = \tilde{k}(T_\infty)$. The calculation of the single-event pre-exponential factors, $\tilde{A}$, is explained in section.

Reactor Model. The calculated molar outlet flow rates, $\hat{F}$, in Eq. 4 are obtained by integrating the continuity equations for all gas-phase species, surface intermediates, and the catalyst. Therefore, appropriate mass balances are derived. The experimental data were collected in a CSTR reactor, in the absence of external and internal transport limitations.[38] Mathematically, solving an initial value problem for a set of ordinary differential equations (ODEs) is much more easy

Table 2. Single-Event Standard Activation Entropies $\Delta \tilde{S}^{0,\ddagger}$ and the Resulting Single-Event Pre-Exponential Factors $\tilde{A}$, Calculated at 723 K and 1 bar Total Pressure, for Each Elementary Reaction Family

Elementary Reaction Family	$\Delta \tilde{S}^{0,\ddagger}$ (J mol^{-1} K^{-1})	$\tilde{A}$ (s^{-1})
Protolytic scission	−95.8	1.96×10^{6}*
Protonation	−95.8	1.96×10^{6}*
Deprotonation	62.2	2.72×10^{16}
Isomerization	0.0	1.51×10^{13}
β-Scission	62.2	2.72×10^{16}
Hydride transfer	−95.8	1.96×10^{6}*

*kPa^{-1} s^{-1}.

than finding the root of a set of nonlinear algebraic equations. Root finding algorithms require a user-supplied initial solution around which the algorithm searches for the real solution. Moreover, the existence of a solution in the region in which the solution in sought is not guaranteed. To overcome these drawbacks, the continuity equations are solved in transient form. The following set of transient continuity equations are valid for the gas-phase species, the surface intermediates, and the catalyst, respectively

$$\frac{dF_i}{dt} = \frac{1}{\tau}\left(F_i^0 - F_i + R_i W\right) \tag{8}$$

$$\frac{dC_{\mathrm{R}_i^+}}{dt} = R_{\mathrm{R}_i^+} \tag{9}$$

$$\frac{dC_*}{dt} = R_* \tag{10}$$

The corresponding initial conditions are $F_i(0) = F_i^0$ for the gas-phase species; $C_{\mathrm{R}_i^+}(0) = 0$ for the carbenium ion intermediates; and $C_*(0) = C_t$ for the catalyst.

In these equations, F_i^0 and F_i are the feed and outlet molar flow rates, respectively; outlet and molar flow rate of species i; R_i, the net rate of formation of species i; W, the catalyst mass; C_t, the total molar concentration of active sites; C_*, the molar concentration of free active sites; $C_{\mathrm{R}_i^+}$, the surface concentration of intermediate R_i^+; t, the time; and τ, the mean residence time in the reactor, calculated as the ratio of the reactor volume (90 cm^3) and the total volumetric inlet flow rate. This set of first-order ODEs is integrated toward steady state to obtain the outlet molar flow rates, F_i, the surface concentrations, $C_{\mathrm{R}_i^+}$, and the molar concentration of free active sites, C_*. The extent of the reaction network and the incorporation of ODEs for the (reactive) intermediates could render the set of equations (8)–(10) stiff. Therefore, the integration is performed using the solver LSODA.[49] It solves the initial value problem for stiff as well as nonstiff systems of first-order ODEs by automatically switching between stiff (backward differentiation formula) and nonstiff methods (Adams).

The net rate of formation of species i, R_i, is calculated by summing over all elementary reaction rates, r, involving species i and is function of the numbers of single events, n_e, the single-event rate coefficients, $\tilde{k}$, the gas phase partial pressures, p_j, the surface concentrations of the intermediates, $C_{\mathrm{R}_i^+}$, and the molar concentration of free active sites, C_*.

The gas phase partial pressure of species j, p_j, is in turn function of the total pressure p_t and the outlet molar flow rates of all species via Eq. (11).

$$p_j = \frac{F_j}{F_{\mathrm{N}_2}^0 + \sum_{k\in\mathrm{gas}} F_k} p_{\mathrm{t}} \tag{11}$$

SEMK Model

The exact nature of the intermediate surface species involved in hydrocarbon conversion processes, alkoxides or carbenium ions, is still a subject of discussion in the literature.[50–56] The SEMK modeling approach describes the conversion of the hydrocarbons based on carbenium ion chemistry that is assumed to occur on the catalyst surface. However, it should be noted that the rate expressions for the elementary steps do not depend on the nature of the intermediates involved, carbenium ions or alkoxides. Based on transition state theory the symmetry contribution related to the structure of the reacting species and the corresponding transition state can be factored out from the elementary rate coefficient k[57] via

$$k = \frac{k_B T}{h}\left(\frac{\sigma_{\mathrm{gl}}^{\mathrm{react}}}{\sigma_{\mathrm{gl}}^{\ddagger}}\right)\exp\left(\frac{\Delta\tilde{S}^{0,\ddagger}}{R}\right)\exp\left(\frac{-\Delta H^{0,\ddagger}}{RT}\right) \tag{12}$$

or

$$k = \frac{\sigma_{\mathrm{gl}}^{\mathrm{react}}}{\sigma_{\mathrm{gl}}^{\ddagger}}\tilde{k} \tag{13}$$

in which k_B, h, and R, are the Boltzmann, Planck, and universal gas constant, respectively; T is the temperature; $\sigma_{\mathrm{gl}}^{\mathrm{react}}$ and $\sigma_{\mathrm{gl}}^{\ddagger}$ are the global symmetry numbers of the reactant and the transition state, respectively; $\Delta\tilde{S}^{0,\ddagger}$ is the standard activation entropy without symmetry contribution; and $\Delta H^{0,\ddagger}$ is the standard activation enthalpy.

The single-event rate coefficient $\tilde{k}$ thus obtained depends only on the reaction family and on the type (primary, secondary, and tertiary) of carbenium ion(s) involved in the elementary step. The ratio of the global symmetry number of the reactant, $\sigma_{\mathrm{gl}}^{\mathrm{react}}$, and the global symmetry number of the transition state, $\sigma_{\mathrm{gl}}^{\ddagger}$, is known as the number of single events, n_e. Because these single-event rate coefficients $\tilde{k}$ depend only on the elementary reaction family and on the types of intermediates involved, they can be estimated based on experimental data acquired from suitable model components such as 2,2,4-trimethylpentane for alkane cracking. In total, 20 single-event rate coefficients $\tilde{k}$ are needed to describe the cracking of alkanes on faujasites.

Reaction network and rate coefficients

The thousands of reactions occurring during catalytic cracking of hydrocarbons can be classified into a limited number of elementary reaction families. These include protolytic scission, (de)protonation, β-scission/alkylation, hydride transfer and isomerization reaction steps. The reaction network is generated automatically using a computer algorithm, where species are represented by vectors and reactions are implemented as simple operations on Boolean relation matrices. Accounting for specific reaction rules, all possible reaction pathways, intermediates and products are generated starting from (a) given feedstock molecule(s).[58,59]

To describe catalytic cracking of acyclics on faujasites only the most stable carbenium ion intermediates are considered, that is, secondary and tertiary. Primary carbenium ions are allowed only to be formed via protolytic scission and to desorb immediately via deprotonation to account for the formation of typical protolytic scission products such as methane, ethane, and ethylene. This reduces the number of elementary steps in the reaction network and also the number of single-event rate coefficients $\tilde{k}$ in the model. Using reversibility concepts for β-scission/alkylation, the number of single-event rate coefficients in the model is further reduced.[37] The number of single-event rate coefficients included in the model to describe catalytic cracking of acyclics on faujasites is limited to 20. These are to be obtained by regression to experimental data. In this work, a separate physisorption step is not explicitly accounted for. It is assumed that a gas phase

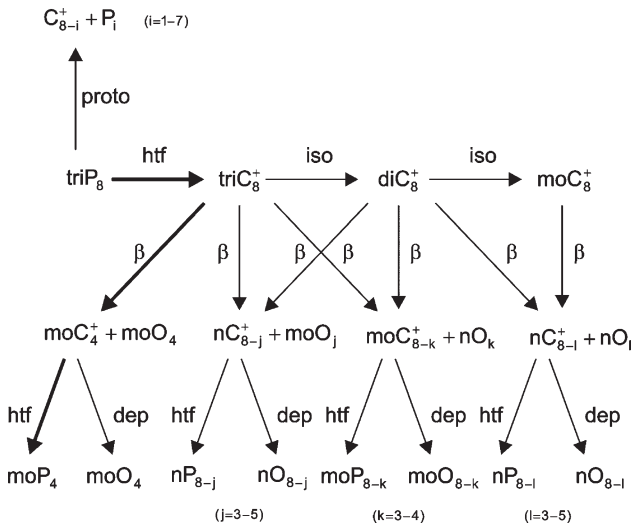

Figure 1. Reaction scheme for catalytic cracking of 2,2,4-trimethylpentane, $triP_8$, on FAU.

nP, moP, and triP represent normal, monobranched, and tribranched alkanes, respectively; nO and moO represent normal and monobranched alkenes, respectively; nC^+, moC^+, diC^+, and $triC^+$ represent normal, monobranched, dibranched, and tribranched carbenium ions, respectively. The terms proto, htf, dep, iso, and β refer to protolytic scission, hydride transfer, deprotonation, isomerization, and β-scission reactions, respectively.

species immediately chemisorbs on a Brønsted acid site upon entering the zeolite pores, thereby forming a carbenium ion intermediate. A justification for this assumption is given in the Supporting Information.

The product distribution obtained when cracking 2,2,4-trimethylpentane over a series of faujasites consists almost entirely of alkanes and alkenes with maximum eight carbon atoms.[38] Figure 1 schematically represents the reaction network explaining the formation of the observed alkanes and alkenes. At all experimental conditions, at most 1 mol % of cyclics and 5 mol % of aromatics were formed. Therefore, it was decided to generate a reaction network consisting only of alkanes, alkenes, and alkylcarbenium ion intermediates with maximum eight carbon atoms. This should be sufficient to evaluate the use of and the identification of appropriate catalyst descriptors in the SEMK model for alkane cracking on faujasites, while keeping the computational cost manageable. The resulting reaction network is summarized in Table 1 and contains in total 231 species: 35 alkanes, 94 alkenes, and 102 alkylcarbenium ions. It comprises 899 reactions: 179 protolytic scissions, 78 hydride transfers, 137 protonations, 88 hydride shifts, 36 methyl shifts, 193 PCP-isomerizations, 21 β-scissions, 6 alkylations, and 161 deprotonations. Using this reaction network, the kinetic parameters involved in catalytic cracking of acyclics on FAU can be determined by regression to the experimental data.

Calculation of the pre-exponential factors

To even further reduce the number of kinetic parameters to be estimated, pre-exponential factors can be calculated a priori combining transition state theory and statistical thermodynamics. This methodology has been applied previously in catalytic cracking by Dumesic and coworkers,[26–28] Klein and coworkers,[30–32] and Quintana-Solórzano et al.[37] It has also been applied in hydrocracking[33,60] and in thermal cracking.[61] The exact calculation of the single-event pre-exponential factors is explained in the Supporting Information.

Table 2 presents the standard activation entropies and the single-event pre-exponential factors of the various hydrocarbon families resulting from these assumptions. One single-event pre-exponential factor is calculated per reaction family. For reaction families involving gas-phase reactants the single event pre-exponential factor has to be divided by the standard state pressure p^0 to provide the correct dimension for $\tilde{A}$.

Results and Discussion

Kinetic descriptors

To describe the cracking of alkanes on faujasites, 20 single-event rate coefficients $\tilde{k}$ need to be determined. To reduce the parameter estimation effort, the corresponding single-event pre-exponential factors $\tilde{A}$ were calculated, leaving 20 activation energies in the SEMK model for acyclics cracking to be estimated by regression to the experimental data obtained on zeolite LZ-Y20. For this catalyst a dataset containing 34 experiments was available, covering a broad range of operating conditions and the widest range of conversion levels, 17–60 mol % (Table 2). This catalyst exhibits an intermediate level of activity compared to the other faujasites.[38] The optimal activation energies and their individual 95% confidence intervals are given in Table 3. The calculated F-value of 2778 is substantially higher than the tabulated one of 2.79 for 4366 degrees of freedom at 95% probability, suggesting that the regression can be considered highly significant. The calculated t-values of the individual parameter estimates, ranging from 8.2×10^2 to 2.2×10^3, are also much higher than the tabulated one of 1.96, implying that each parameter is significantly different from zero. High t-values lead to narrow confidence intervals, as can be

Table 3. Estimated Activation Energies in kJ mol^{-1} and Their Individual 95% Confidence Intervals for the Elementary Reaction Families and Types Included in the SEMK Model Describing Catalytic Cracking of Acyclics on Zeolite LZ-Y20

	Reaction Type			
Reaction Family	p	s	t	
Protolytic scission	140.1 ± 0.2	156.4 ± 0.3	156.5 ± 0.4	
Protonation		96.7 ± 0.1	80.5 ± 0.1	
Deprotonation	116.0 ± 0.2	187.0 ± 0.3	199.5 ± 0.3	
Hydride transfer		111.4 ± 0.2	112.0 ± 0.1	
	(s;s)	(s;t)	(t;s)	(t;t)
Hydride/methyl shift	70.9 ± 0.1	67.2 ± 0.1	95.9*	85.7 ± 0.1
PCP-isomerization	118.6 ± 0.2	113.0 ± 0.1	141.7*	119.6 ± 0.2
β-Scission	126.3 ± 0.2	118.7 ± 0.2	154.2 ± 0.3	139.6 ± 0.2

*Calculated via $E_{a,iso}(t;s) = E_{a,iso}(s;t) + \Delta H_{pr}(s) - \Delta H_{pr}(t)$.

Table 4. Activation Energies in kJ mol^{-1} Reported in the Literature for Catalytic Cracking and Hydrocracking of Alkanes on Faujasites

	Catalytic Cracking			Hydrocracking		
Reaction Type	Ref. 28	Ref. 29	Ref. 62	Ref. 37	Ref. 33*	Ref. 63
$E_{a,proto}(p)$				145		
$E_{a,proto}(s)$	159–166	130–181	154	162		
$E_{a,proto}(t)$		144–266		169		
$E_{a,pr}(s)$	−75†	−80†		114		−65†
$E_{a,pr}(t)$	−150‡	−150‡		95		−96‡
$E_{a,dep}(p)$				75		
$E_{a,dep}(s)$				169		
$E_{a,dep}(t)$				215		
$E_{a,htf}(s)$	115–147	123–136		134		
$E_{a,htf}(t)$	66–122	48–110	62–77	61		
$E_{a,hs/ms}(s;s)$			80			77
$E_{a,hs/ms}(s;t)$			80			74
$E_{a,hs/ms}(t;s)$	74	76	80			105
$E_{a,hs/ms}(t;t)$			80			105
$E_{a,pcp}(s;s)$			110	134	134	109
$E_{a,pcp}(s;t)$			110	71	127	99
$E_{a,pcp}(t;s)$	78	74–84	110	145	155	129
$E_{a,pcp}(t;t)$			110	177	151	128
$E_{a,\beta}(s;s)$		131–169	115	238	160	143
$E_{a,\beta}(s;t)$		152	115	161	147	128
$E_{a,\beta}(t;s)$	73	202		198	174	149
$E_{a,\beta}(t;t)$	187		102	243	148	125

†$\Delta H_{pr}(s)$.
‡$\Delta H_{pr}(t)$.
*The composite activation energies reported by these authors are converted into true activation energies using the protonation enthalpies obtained in this work; −90.3 and −119.0 kJ mol^{-1} toward secondary and tertiary alkylcarbenium ions, respectively.

observed in Table 3. The binary correlation coefficients are lower than 0.74, in absolute values, indicating that the parameter estimates were not correlated.

Except for protolytic scission and hydride transfer reactions, all estimated activation energies are in accordance with the stability of the carbenium ion intermediates involved. Formation of a tertiary carbenium ion via protonation of an alkene requires a lower activation energy than the formation of a secondary intermediate. In contrast, deprotonation of a highly unstable primary carbenium ion will occur much faster than that of a secondary, which is in turn faster than that of a tertiary. Furthermore, activation energies of reactions converting tertiary carbenium ions are significantly higher than the activation energies of reactions converting secondary carbenium ions. For isomerization and β-scission reactions, reaction rates of $(s;t)$ surface reactions are higher than those of the corresponding $(s;s)$ type. Similarly, reaction rates of $(t;s)$ surface reactions are lower than those of the corresponding $(t;t)$ type. For hydride transfer reactions, the activation energy is essentially independent of the nature of the intermediates involved, leading to practically equal activation energies of hydride transfer reactions converting gas-phase alkanes into secondary and into tertiary intermediates. For protolytic scission, the activation energy for the formation of primary carbenium ions is somewhat lower than those of secondary and tertiary ones, for which an equal activation energy was estimated. However, protolytic scission via primary carbenium ions plays only a minor role in the observed product distribution.

Activation energies reported in other detailed mechanistic studies on catalytic cracking and hydrocracking of alkanes on faujasites are presented in Table 4. Dumesic and coworkers investigated catalytic cracking of isobutane[28,62] and 2-methylhexane[29] over several USY zeolites with varying acid properties, Quintana-Solórzano et al.[37] studied catalytic cracking of a mixture of *n*-decane and 1-octene over a USY-based equilibrium catalyst, whereas Martens et al.[33] and Thybaut et al.[63] examined hydrocracking of *n*-alkanes on Pt/USY zeolites. The estimated activation energies of protolytic scission, ranging from 140 to 157 kJ mol^{-1}, are very similar to those reported by Yaluris et al.,[28] Sanchez-Castillo et al.,[62] and Quintana-Solórzano et al.,[37] and fall into the relatively wide range of activation energies mentioned by Yaluris et al.[29] Corma et al.[64] reported activation energies of protolytic scission of isobutane on USY in the range 160–170 kJ mol^{-1}.

The protonation enthalpy toward secondary carbenium ions corresponds to −90.3 kJ mol^{-1}, while the protonation enthalpy toward tertiary intermediates amounts to −119.0 kJ mol^{-1}. This results in a higher concentration of tertiary surface intermediates than secondary ones. The difference in stability between secondary and tertiary carbenium ions thus amounts to 28.7 kJ mol^{-1}. This is slightly below the enthalpy difference of 40–60 kJ mol^{-1} between secondary and tertiary ions in liquid superacids.[65–67] Also, the protonation enthalpy toward secondary carbenium ions is somewhat higher, in absolute value, than those reported in the literature (see Table 4), whereas that toward tertiary carbenium ions lies between the values of −96 and −150 kJ mol^{-1} found by Thybaut et al.[63] and Yaluris et al.,[28,29] respectively.

For hydride transfer reactions, the activation energies reported in Table 4 differ widely. Yaluris et al.[28,29] and Quintana-Solórzano et al.[37] estimated higher activation energies of hydride transfer reactions forming secondary intermediates than those forming tertiary, whereas Beirnaert et al.[36] reported equal activation energies for both reaction types.

The activation energies of isomerization reactions agree rather well with those reported by Martens et al.[33] and Thybaut et al.[63] In this work, activation energies of nonbranching isomerizations are some 40 kJ mol^{-1} lower than those of branching rearrangements, which is somewhat higher than the difference of about 30 kJ mol^{-1} reported by Sanchez-Castillo et al.[62] and Thybaut et al.[63] However, in the latter study, only methyl shifts were accounted for, not hydride shifts, which are included in this work. A DFT-study on the isomerization reactions of hexyl species involved in the conversion of 2-methyl-2-pentene via alkoxide intermediates on an aluminosilicate cluster revealed activation energies of hydride shift, methyl shift, and PCP-isomerization of 52, 71, and 117 kJ mol^{-1}, respectively.[68] Kramer et al.[69] studied isomerization of 2-methyl-2-pentene on USY and measured activation energies of hydride shift and methyl shift around 47 and 63 kJ mol^{-1}, respectively.

For β-scission reactions, the activation energies presented in Table 4 differ widely. The activation energies estimated in this work agree rather well with those reported by Thybaut et al.,[63] whereas those mentioned by Martens et al.[33] are slightly higher.

Figure 2 illustrates the agreement between the measured and model calculated molar outlet flow rates when cracking 2,2,4-trimethylpentane on reference zeolite LZ-Y20. All 129 responses taken into account in the objective function are represented to indicate that also the unobserved responses are described correctly. This overall parity plot shows that the kinetic model is able to describe the experimental data reasonably well. A more detailed evaluation of the model calculations is given in Figure 3 that shows model simulation results describing the selectivities of the most abundant

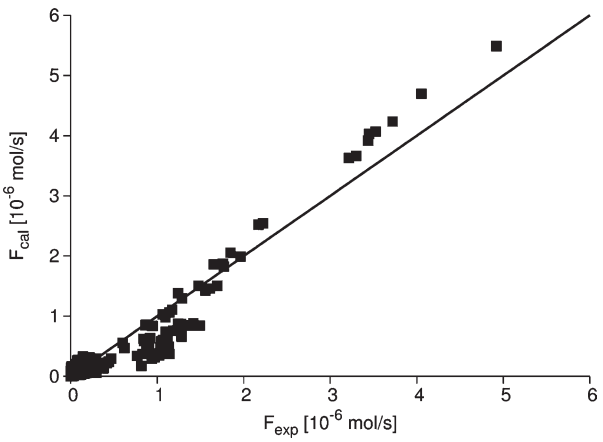

Figure 2. Calculated vs. experimental molar outlet flow rates of all gas phase hydrocarbons in the reaction network accounted for in the model describing catalytic cracking of acyclics on reference catalyst LZ-Y20.

Model calculated values are obtained from solving Eqs. 8–10 and using the pre-exponential factors in Table 2 and the activation energies in Table 3. Experimentally observed values are obtained from 2,2,4-trimethylpentane cracking at T = 698–748 K, p_{iC8} = 6–15 kPa, and W/F^0_{iC8} = 8–90 kg s mol^{-1}.

cracking products of 2,2,4-trimethylpentane on LZ-Y20 as a function of conversion, at 748 K and 7 kPa. As can be observed, the trends for propane, isopentane, isobutene, and *n*-butane are reasonably well described by the kinetic model. For propylene, isobutane, and 2-butene the discrepancy between the measured and the calculated selectivities is somewhat larger. The selectivities of typical protolytic scission products (not represented) such as ethane and ethylene are described correctly, whereas that of methane is slightly overestimated. Also at other experimental conditions, the agreement between the experimental product selectivities and the calculated ones is reasonable. The predictive capabilities of the model will be improved by extending the reaction network to incorporate alkylation reactions toward higher carbon number intermediates that recrack via β-scission into C_3—C_5 alkanes and alkenes. However, the computational cost will increase drastically (Table 2).

At the conditions tested (see Table 2), the calculated fractional coverage of the catalyst active sites with surface intermediates ranges from 4.0×10^{-3} to 3.1×10^{-2}. The coverage of the catalyst is determined by the rates of the elementary reactions forming intermediates, that is, protolytic scission and protonation, and the rates of reactions consuming intermediates, that is, deprotonation. Lower fractional coverages are found at lower conversion, at lower partial pressure, and at higher reaction temperature. The latter is explained by the high activation energy of the deprotonation step, rendering desorption more difficult at low temperature. Around 80% of these surface intermediates are of tertiary nature, of which ~75% are *t*-butyl ions and ~25% correspond to 2-methyl-2-butyl ions. The other 20% of surface intermediates are of secondary nature, mainly 2-propyl, and 2-butyl. The calculated concentrations of these surface species are entirely in agreement with what could be expected based on the product distribution obtained. Over the whole conversion range, the main cracking products of 2,2,4-trimethylpentane are isobutane, isobutene, 2-butene, propylene, and isopentane.[38] Figure 4 represents the calculated fractional surface coverage with intermediates as a function of the reactant partial pressure and the temperature. At partial pressures above 9 kPa, the fractional coverage rapidly increases, especially at lower temperatures.

Introduction of acidity descriptors in the SEMK model

To describe the effect of the acid properties of the zeolite on the observed catalytic behavior, the appropriate catalyst descriptors are introduced in the kinetic model. The catalyst acidity is controlled by the concentration of acid sites and their average acid strength. Variations in the number of active sites are easily accounted for via altering C_t, which is commonly measured via techniques such as NH_3-TPD. However, accounting for changes in the acid strength of the active sites is less straightforward, and the corresponding catalyst descriptors are to be obtained by regression.

So far, only a few kinetic models that explicitly account for the effect of the strength of the acid sites have been reported in the literature. Dumesic and coworkers[26–29] have incorporated a single adjustable parameter, ΔH_+, in their kinetic model to describe the effect of acid strength on the cracking of isobutane or 2-methylpentane on a series of USY zeolites. Klein and coworkers[30–32] applied the same approach to the cracking of various hydrocarbons on FAU or MFI zeolites. The parameter ΔH_+, given in Eq. 14, reflects the heat of stabilization of a carbenium ion relative to the heat of stabilization of a proton on the acid site and is assumed to be independent of the carbenium ion involved. It is also equal to the heat of formation of a surface carbenium ion by reaction of a gas-phase alkene with a Brønsted acid site relative to the heat of formation of a gas-phase carbenium ion by reaction of an alkene with a gas-phase proton. The physical meaning of ΔH_+ can be understood from the thermodynamic cycle in Figure 5. The following relationship can be derived

$$\Delta H_+ = \Delta H^0_{\mathrm{pr,zeo}} - \Delta H^0_{\mathrm{pr,gas}} = \Delta H^0_{\mathrm{stab,R^+}} - \Delta H^0_{\mathrm{stab,H^+}} \quad (14)$$

where $\Delta H^0_{\mathrm{pr,zeo}}$ and $\Delta H^0_{\mathrm{pr,gas}}$ represent the standard enthalpies of protonation by the zeolite and in the gas phase, respectively; and $\Delta H^0_{\mathrm{stab,R^+}}$ and $\Delta H^0_{\mathrm{stab,H^+}}$ represent the standard enthalpies of stabilization of the carbenium ion and of the proton by the zeolite, respectively. The latter is equal to the proton affinity of the zeolite anion ZeO^-, PA_{ZeO^-}. In Eq. 14, only the term $\Delta H^0_{\mathrm{pr,gas}}$ is catalyst independent. For a series of USY zeolites, estimates for ΔH_+ were obtained ranging from 686 to 718 kJ mol^{-1}.[26–29]

In our research group, kinetic models explicitly accounting for acid strength have been developed for hydroconversion of alkanes on Pt/USY zeolites.[33,34] In alkane hydrocracking, a single catalyst dependent adjustable parameter, $\Delta(\Delta H^0_{\mathrm{pr}})$, is introduced to account for the effect of average acid strength on the composite activation energies. This parameter $\Delta(\Delta H^0_{\mathrm{pr}})$ reflects the difference in standard protonation enthalpy between two catalysts, A and B, via

$$\Delta(\Delta H^0_{\mathrm{pr}}) = \Delta H^0_{\mathrm{pr,B}} - \Delta H^0_{\mathrm{pr,A}} \quad (15)$$

Comparing Eqs. 14 and 15 shows that this approach is equivalent to that of Dumesic and coworkers,[26–29] because also

$$\Delta(\Delta H^0_{\mathrm{pr}}) = \Delta H_{+,\mathrm{B}} - \Delta H_{+,\mathrm{A}} \quad (16)$$

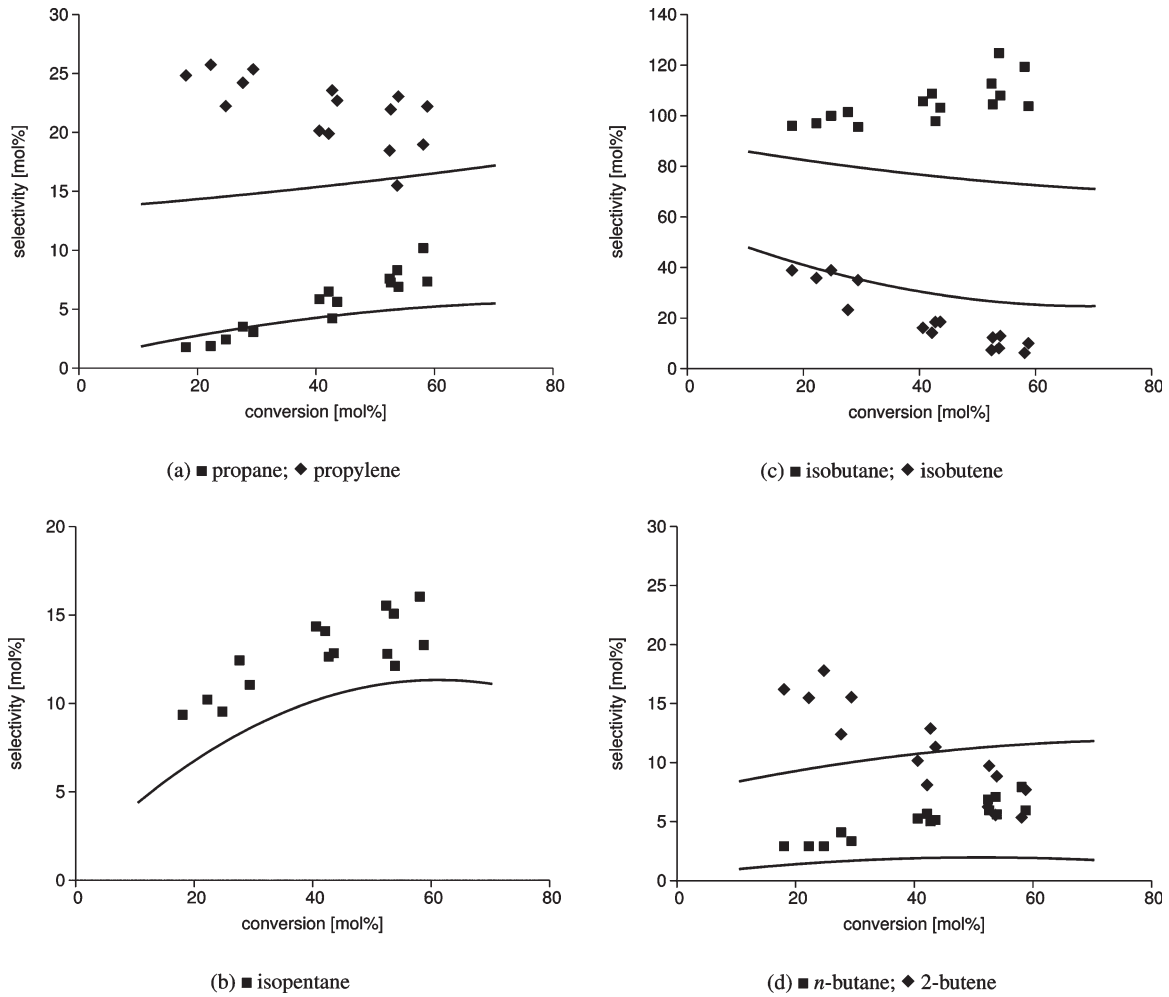

Figure 3. Experimental (symbols) vs. calculated (lines) selectivities of the main cracking products of 2,2,4-trimethylpentane as a function of conversion on reference zeolite LZ-Y20 at 748 K and 7 kPa partial pressure.

The solid lines represent model calculated results obtained from solving Eqs. 8–10 and using the pre-exponential factors in Table 2 and the activation energies in Table 3.

In liquid-phase alkylation of benzene with 1-octene on USY zeolites,[70] the influence of the average acid strength of the catalyst was evaluated using two catalyst-dependent parameters, α and $\Delta(\Delta H^0_{pr})$. Analogous to Eq. 15, the change in standard protonation enthalpy, $\Delta(\Delta H^0_{pr})$, accounts for the stabilizing effect of the zeolite on the intermediates. Applying the Evans–Polanyi principle, the stabilizing effect of the zeolite on the transition state will be related to that of the intermediates via a factor α.

In principle, the effect of the zeolite acid strength on the observed catalytic behavior can be related to energetic contributions, entropic contributions, or both. Recently, Bhan et al.[15] pointed at the importance of the intrinsic pre-exponential factors in explaining observed activity and selectivity differences on monomolecular cracking of alkanes on zeolites. In this work, catalytic cracking is limited to faujasites with varying acid properties, and it can be assumed that the entropic contribution will be similar for all of them. Thus, to incorporate the effect of acidity a kinetic modeling approach similar to that of Dumesic and coworkers[26–29] and Klein and coworkers[30–32] for catalytic cracking and that of Martens et al.[33] and Thybaut et al.[34] for hydrocracking is taken.

To illustrate the effect of the zeolite acid strength on the elementary steps occurring during catalytic cracking, Figure 6 represents the energy diagram of a reaction pathway, consisting of protonation of a gas-phase alkene by the zeolite, followed by a PCP-isomerization of the reaction intermediate

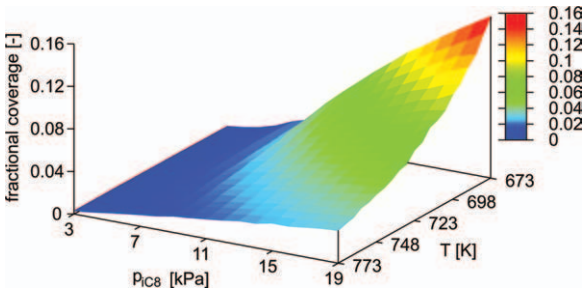

Figure 4. Fractional surface coverage with intermediates on reference catalyst LZ-Y20 as a function of the partial pressure and the temperature, at a space time of 41.4 kg s mol^{-1} and a total pressure of 102 kPa, obtained from solving Eqs. 8–10, and using the pre-exponential factors in Table 2 and the activation energies in Table 3.

[Color figure can be viewed in the online issue, which is available at wileyonlinelibrary.com.]

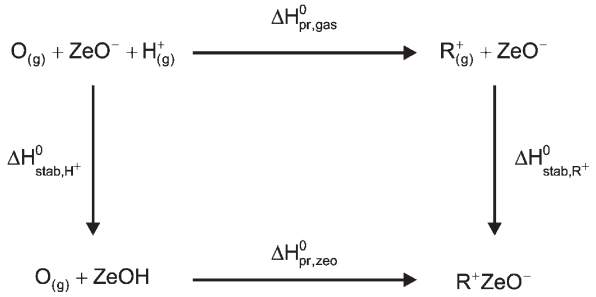

Figure 5. Hypothetical thermodynamic cycle representing the various contributions for protonation of a gas-phase alkene O into a carbenium ion R^+ by the zeolite ZeOH.

into a second intermediate, taking place on two catalysts, A and B. The activation energies of both steps are indicated as $E_{a,pr}$ and $E_{a,pcp}$, respectively, whereas ΔH^0_{pr} represents the protonation enthalpy. The latter is related to the deprotonation activation energy via Eq. 17.

$$E_{a,pr} - \Delta H^0_{pr} = E_{a,dep} \tag{17}$$

In general, these energy levels can be expected to shift downward when the reaction pathway occurs on a zeolite with higher acid strength, catalyst B in Figure 6. The intermediates as well as the transition states will be stabilized by the zeolite to a larger extent than on catalyst A, leading to changes in the protonation enthalpy, $\Delta(\Delta H^0_{pr})$, and/or in the activation energies, ΔE_a, given by Eqs. 15 and 18, respectively.

$$\Delta E_a = E_{a,B} - E_{a,A} \tag{18}$$

Depending on the nature of the surface intermediates, different situations can arise. In case the surface intermediates are carbenium ions, the transition state as well as the intermediate itself have full ionic character. As a result, the stabilizing effect of the zeolite on the intermediates and the transition states can be expected to be similar. All energy levels in Figure 6 are then expected to shift to the same extent by an amount $\Delta(\Delta H^0_{pr})$. In case the surface intermediates are neutral alkoxides and the transition states are positively charged carbenium ions, the stability of the intermediates can be expected to remain quasi unaffected by the zeolite acid strength, while the stability of the transition states will alter. In that case, only the energy levels of the transition states are expected to shift. Quantum-chemical calculations have revealed that the more pronounced the ionic character of the transition state is, that is, the higher the charge separation, the more sensitive the corresponding reaction pathway is to variations in acid strength.[68] This implies that activation energies of reaction pathways that are affected by the zeolite acidity to a different extent will alter in a different manner. The real situation may be situated between these two extreme cases, with the intermediate having a partial ionic charge that turns into a more positively charged transition state during reaction. In that case, variations in acid strength are expected to result in changes in the stability of the intermediates as well as the transition states. Assuming that the stabilization of the intermediate by the zeolite is independent of its primary, secondary, or tertiary nature allows to introduce one parameter, $\Delta(\Delta H^0_{pr})$, accounting for the effect of acid strength on the stability of the intermediates. Assuming that the stabilization of the transition state is also independent of the primary, secondary, or tertiary nature of the reactant and/or product intermediates allows to introduce one parameter, ΔE_a, per reaction family, accounting for the effect of acid strength on the stability of the corresponding transition states. These catalyst descriptors are determined relative to a reference catalyst. If catalyst B in Eqs. 15 and 18 is chosen as the reference catalyst, that is, LZ-Y20, positive values of $\Delta(\Delta H^0_{pr})$ and ΔE_a correspond to a zeolite with higher acid strength than the reference catalyst.

Experimentally, only differences in activity were observed, not in selectivity, when cracking 2,2,4-trimethylpentane on these five faujasites.[38] A unique relationship was found between the product selectivities and conversion, independent of the acid properties of the zeolites, indicating that within this series of faujasites, the acid properties only control the cracking activity, but not the selectivity. The absence of selectivity differences indicates that each reaction pathway in the reaction network must be affected by variations in acid strength in the same way. Any reaction pathway involved in the cracking of hydrocarbons on a zeolite active site consists of an adsorption step to form a surface intermediate, protolytic scission for alkanes or protonation for alkenes, a number of surface reactions interconverting intermediates, such as isomerization, β-scission, alkylation, and hydride transfer, and finally a desorption step via deprotonation to restore the active site. As explained above, a change in acid strength of the zeolite will result in a change in the stability of the surface intermediates by an amount $\Delta(\Delta H^0_{pr})$. When each reaction pathway is to be affected to the same extent by changes in acid strength, Eqs. 19 and 20 must be valid concerning the effect of acid strength on the stability of the corresponding transition states of surface reactions and adsorption reactions, respectively.

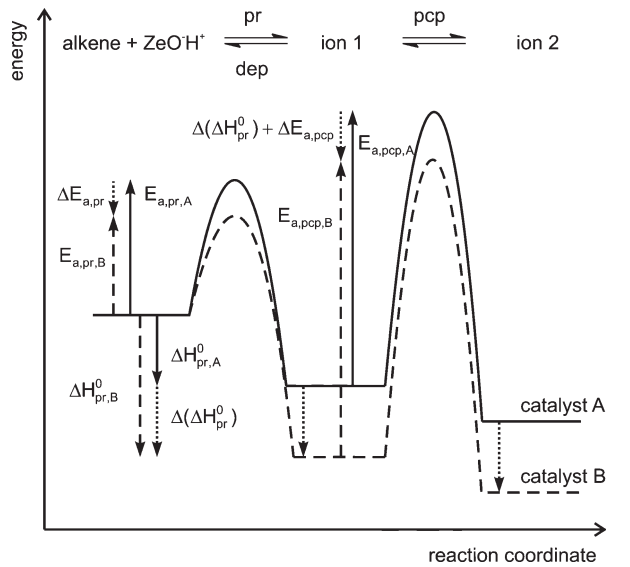

Figure 6. Energy diagram for protonation of a gas-phase alkene by the zeolite, followed by PCP-isomerization.

Solid line: catalyst A; dashed line: catalyst B; dotted line: acidity descriptors. $E_{a,pr}$ and $E_{a,pcp}$, correspond to the activation energies of the protonation and the isomerization step, respectively; ΔH^0_{pr} represents the standard protonation enthalpy.

Table 5. Estimated Changes in Standard Protonation Enthalpy Relative to the Reference Catalyst LZ-Y20 in kJ mol^{-1}, 95% Confidence Intervals, Significance of the Parameter Estimate, and Significance of the Global Regression

Zeolite	Δ (ΔH^0_{pr})	t-Value	F-Value
CBV500	5.42 ± 0.15	72	1.28×10^4
CBV720	3.07 ± 0.14	43	2.64×10^4
CBV760	0.95 ± 0.03	55	1.72×10^5
Y62	−23.48 ± 0.10	−457	1.94×10^6

$$\Delta E_{a,iso} = \Delta E_{a,htf} = \Delta E_{a,\beta} \tag{19}$$

$$\Delta E_{a,pr} = \Delta E_{a,proto} \tag{20}$$

As the number of surface reactions in a reaction pathway is variable, for example, converting 2,2,4-trimethylpentane into isobutene does not require any isomerization reaction, while at least one isomerization reaction is necessary to produce 2-pentene (see Figure 1), Eq. 19 must also be equal to zero. This means that for the surface reactions, the intermediates and the transition states are stabilized by the zeolite to the same extent, $\Delta(\Delta H^0_{pr})$, such that the corresponding activation energies do not change when varying the acid strength. Analogously, Eq. 20 states that the activation energies of protolytic scission and protonation are affected to the same extent by variations in acid strength. It can reasonably be assumed that the transition states of adsorption reactions will be stabilized by the zeolite to the same extent, $\Delta(\Delta H^0_{pr})$, as the transition states of the surface reactions, leading to Eq. 21.

$$\Delta E_{a,pr} = \Delta E_{a,proto} = \Delta(\Delta H^0_{pr}) \tag{21}$$

To summarize, the effect of acidity can be included in the SEMK model using only two acidity descriptors: the concentration of active sites, C_t, and the change in standard protonation enthalpy, $\Delta(\Delta H^0_{pr})$, relative to a reference catalyst (Table 1). The latter parameter accounts for the effect of the average acid strength on the stability of the intermediates and on the activation energies of protonation and protolytic scission. The concentration of acid sites is available from NH_3-TPD measurements (Table 1), while the change in standard protonation enthalpy relative to the reference catalyst LZ-Y20 must be obtained by regression to the experimental data.

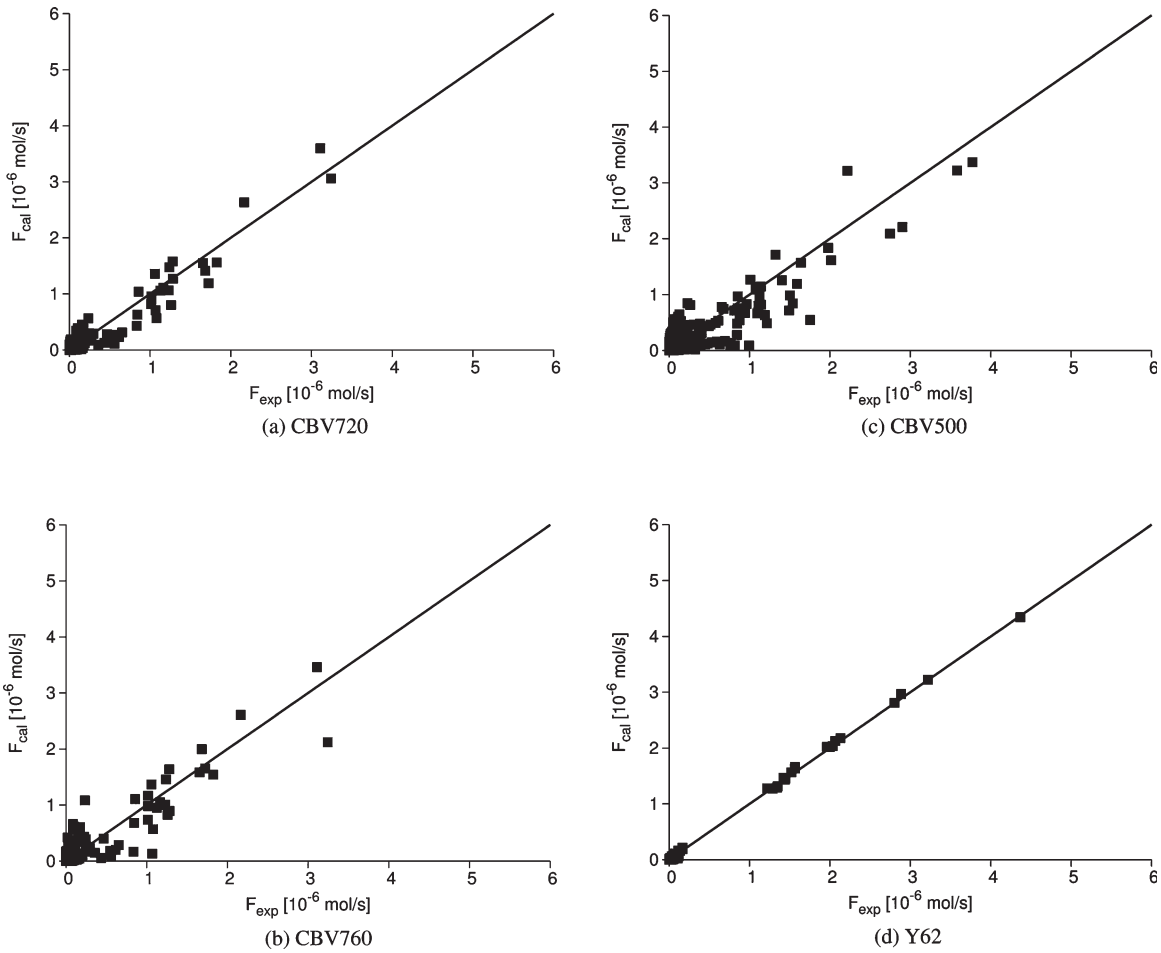

Figure 7. Calculated vs. experimental molar outlet flow rates of all gas-phase hydrocarbons in the reaction network accounted for in the model describing catalytic cracking of acyclics on CBV720, CBV760, CBV500, and Y62.

Model calculated values are obtained from solving Eqs. 8–10 and using the pre-exponential factors in Table 2, the activation energies obtained on the reference catalyst LZ-Y20 in Table 3, the concentration of active sites in Table 1 and the change in standard protonation enthalpy in Table 5. Experimentally observed values are obtained from 2,2,4-trimethylpentane cracking under the conditions given in Table 2.

Table 5 represents the estimated changes in standard protonation enthalpy relative to the reference catalyst LZ-Y20 and the corresponding statistical information concerning the significance of the parameter estimate and that of the global regression. Because $\Delta(\Delta H^0_{pr}) = \Delta H^0_{pr,LZ-Y20} - \Delta H^0_{pr,zeo}$, positive values correspond to a zeolite with higher acid strength than LZ-Y20, whereas negative values correspond to a zeolite with lower acid strength. In this series of faujasites, CBV500 displays the highest acid strength, whereas Y62 exhibits by far the lowest one. The four ultrastable Y zeolites possess rather similar acid strengths, because the difference in standard protonation enthalpy amounts to 5.4 kJ mol^{-1} at most. This is in agreement with the experimental data.[38] As can be observed from the narrow confidence intervals and the *t*-values, which are all higher (in absolute value) than the tabulated *t*-value of 1.96, the estimated changes in standard protonation enthalpy are all statistically significant. The reported *F*-values are all much higher than the tabulated one of 4.84, indicating that the global regression is highly significant.

The range of standard protonation enthalpy variation around 29 kJ mol^{-1} found in this work agrees very well with the range of 26 kJ mol^{-1} found by Yaluris et al.[29] for cracking of 2-methylpentane on a series of USY zeolites with Si/Al ratio ranging from 10 to 80. Thybaut et al.[34] found a change in standard protonation enthalpy between a Y zeolite with Si/Al ratio of 2.6, Pt/CBV720, and Pt/CBV760 (reference) around −18.1 and 3.5 kJ mol^{-1}, respectively. These values agree rather well with those found in this work. Martens et al.[33] found a difference in standard protonation enthalpy of 2.1 kJ mol^{-1} between two commercial hydrocracking catalysts derived from LZ-Y20.

Figure 7 illustrates the agreement between the measured and the calculated molar outlet flow rates. The latter values are obtained using the pre-exponential factors in Table 2, the activation energies obtained on the reference catalyst LZ-Y20 in Table 3, and the two acidity descriptors C_t in Table 1 and $\Delta(\Delta H^0_{pr})$ in Table 5. The overall parity plots indicate that the model including two acidity descriptors describes the experimental data reasonably well, especially for Y62, which could be expected from the very high *F*-value (Table 5).

To illustrate the ability of the model to predict the absence of selectivity differences when varying the zeolite acid strength, Figure 8 represents the model calculated product selectivities toward isobutene and isopentane as a function of 2,2,4-trimethylpentane conversion on all five faujasites at 748 K and 7 kPa partial pressure. The calculated trends are identical for the five faujasites, indicating that introducing C_t and $\Delta(\Delta H^0_{pr})$ as catalyst descriptors in the model, indeed allows to describe correctly the observed effect on activity and selectivity when cracking 2,2,4-trimethylpentane on a series of faujasites with varying acid properties. The discrepancies between the model calculated and the experimental product selectivities could be reduced by extending the reaction network to include species with higher carbon number than the feed, formed via alkylation, which subsequently recrack.

Figure 9 represents the fractional surface coverage with intermediates for CBV500, CBV720, CBV760, and Y62 as a function of the partial pressure and the temperature. The increased surface coverage with higher acid strength is evident. The fractional coverage is much higher on the three USY zeolites compared to that on the Y zeolite. Moreover, the dependence on the temperature is inversed on Y62. This

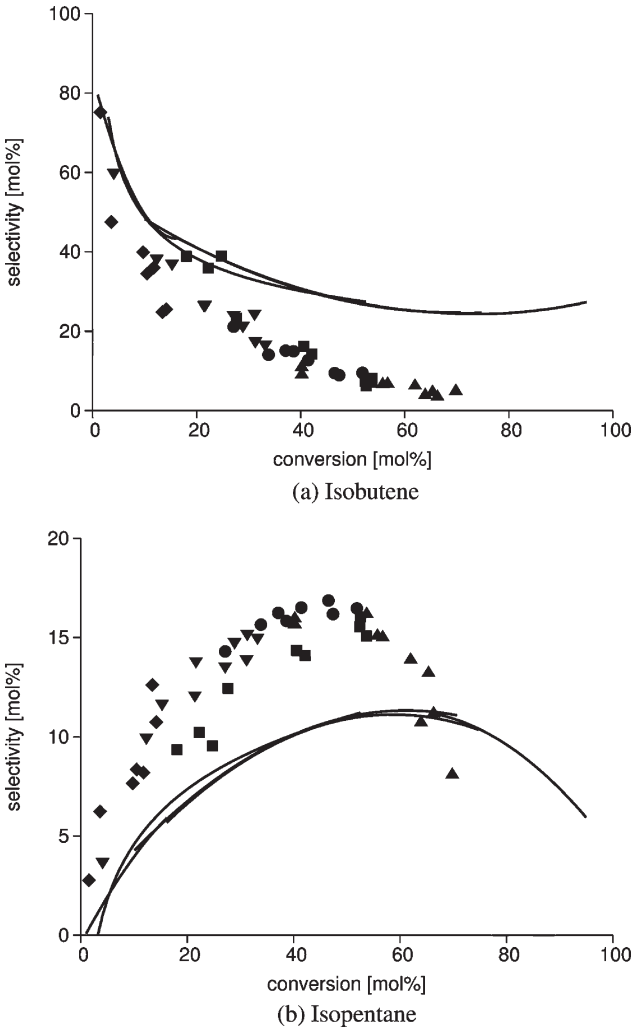

Figure 8. Experimental (symbols) and model calculated (lines) product selectivities as a function of 2,2,4-trimethylpentane conversion on five faujasites, at 748 K and 7 kPa partial pressure.

Experimental: (◆) Y62; (■) LZ-Y20; (▲) CBV500; (●) CBV720; (▼) CBV760. Model calculated values are obtained from solving Eqs. 8–10 and using the pre-exponential factors in Table 2, the activation energies obtained on the reference catalyst LZ-Y20 in Table 3, the concentration of active sites in Table 1 and the change in standard protonation enthalpy in Table 5.

is explained by the (very) low conversion on this zeolite, at which the surface coverage is determined by the activation energy of protolytic scission instead of that of deprotonation.

Conclusions

The SEMK modeling approach can be applied to develop a kinetic model that can account for the effect of the zeolite acid properties when cracking alkanes on faujasites in the absence of coke formation. Data obtained on 2,2,4-trimethylpentane cracking can be described adequately with standard activation entropies for the various elementary reaction families calculated *a priori* based on transition state theory and statistical thermodynamics. Activation energies on the reference faujasite LZ-Y20 for the various types of protolytic

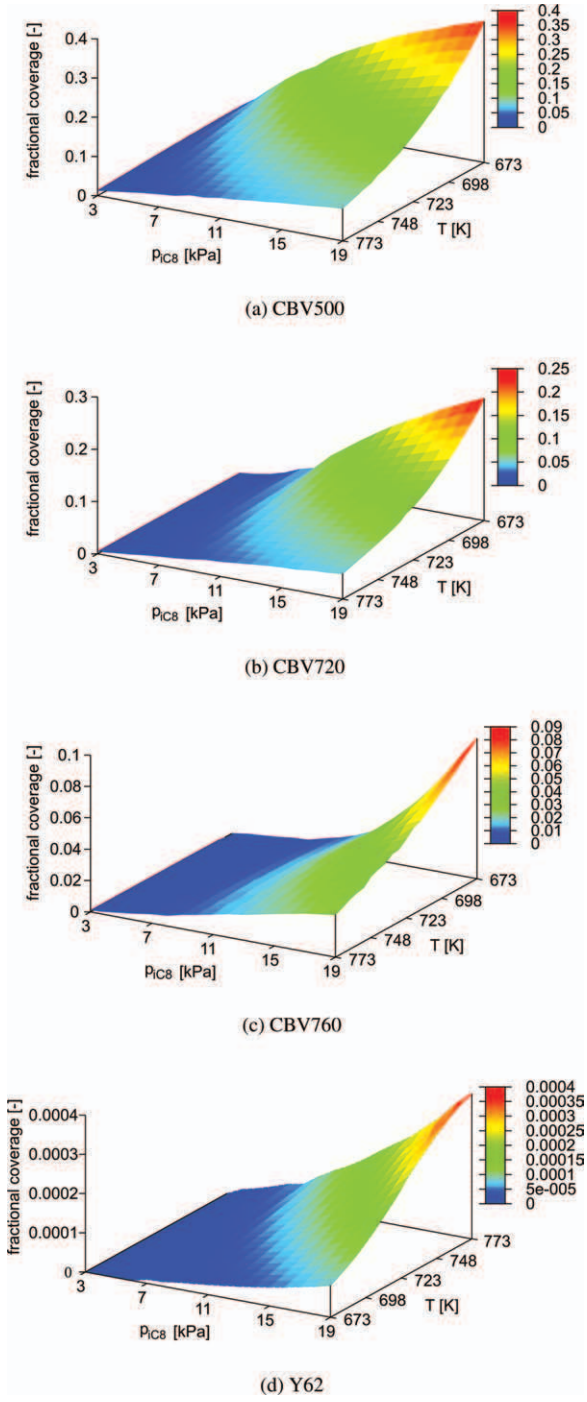

Figure 9. Fractional surface coverage with intermediates on faujasites as a function of the partial pressure and the temperature, at a space time of 41.4 kg s mol^{-1} and a total pressure of 102 kPa, obtained from solving Eqs. 8–10, and using the pre-exponential factors in Table 2, the activation energies in Table 3, the concentration of active sites in Table 1 and the change in standard protonation enthalpy in Table 5.

[Color figure can be viewed in the online issue, which is available at wileyonlinelibrary.com.]

scission, protonation, deprotonation, hydride transfer, hydride shift, methyl shift, PCP-isomerization, and β-scission can be obtained via regression to experimental kinetic data. The model describes the experimentally observed trends reasonably well. The estimated activation energies are in accordance with the stability of the intermediates involved, except for protolytic scission toward primary intermediates and hydride transfer. A difference in stability between secondary and tertiary intermediates of 28.7 kJ mol^{-1} is obtained, resulting in a higher concentration of tertiary surface intermediates than secondary ones, ~80% of the former vs. ~20% of the latter type. Lower fractional surface coverages are found at lower conversion, at lower partial pressure, and at higher reaction temperature.

It was sufficient to incorporate two acidity descriptors in the model to describe the effect of variations in acidity on the observed catalytic behavior: the concentration of active sites, C_t, which is available from independent NH_3-TPD measurements, and the change in standard protonation enthalpy relative to a reference catalyst, $\Delta(\Delta H^0_{pr})$, which is determined by regression to experimental data on four other commercial faujasites. The entropic contribution is assumed to be similar for all faujasites. The intermediates and the transitions states are stabilized by the zeolite in the same way by an amount $\Delta(\Delta H^0_{pr})$. Thus, the activation energies of protonation and protolytic scission change, while those of surface reactions and deprotonation remain equal when varying the acid strength. The change in protonation enthalpy relative to the reference faujasite accounts for the effect of the average acid strength both on the stability of the intermediates and on the activation energies of protonation and protolytic scission. The model is capable of describing the observed effects of variations in acidity. A variation in standard protonation enthalpy of 29 kJ mol^{-1} was found for the five faujasites. The acid strength of the four ultrastable faujasites is rather similar and much higher than that of the nondealuminated Y zeolite. Increasing the acid strength results in a higher fractional surface coverage with intermediates.

At the conditions of this work, the concentration of physisorbed species is negligible compared to the total concentration of active sites and to the fractional coverage with surface intermediates. Physisorption can thus be considered kinetically insignificant and the hydrocarbons will effectively chemisorb upon entering the zeolite without a preceeding physisorption step. Consequently, differences in physisorption properties cannot account for observed differences in activity between the faujasites.

Acknowledgments

The Institute for the Promotion of Innovation through Science and Technology in Flanders (IWT-Vlaanderen) is gratefully acknowledged for their financial support to the SBO 030202 project. The Belgian government is acknowledged by the authors for supporting an IAP-PAI network and the Flemish government for long-term structural funding (Methusalem).

Notation

$\tilde{A}$ = single-event pre-exponential factor, s^{-1} or kPa^{-1} s^{-1}
$\tilde{A}_{rep}$ = reparameterized single-event pre-exponential factor, s^{-1} or kPa^{-1} s^{-1}
$\boldsymbol{b}$ = vector of the estimated model parameters
C_* = molar concentration of free active sites, mol kg$_{cat}^{-1}$
$C_{R_i^+}$ = molar concentration of intermediate R_i^+, mol kg$_{cat}^{-1}$
C_t = total molar concentration of active sites, mol kg$_{cat}^{-1}$
E_a = activation energy, J mol^{-1}
F_i = molar flow rate of species i, mol s^{-1}
h = Planck constant, J s

k = elementary rate coefficient, s^{-1} or $kPa^{-1}\ s^{-1}$
$\tilde{k}$ = single-event rate coefficient, s^{-1} or $kPa^{-1}\ s^{-1}$
$\tilde{K}_{iso}$ = single-event isomerization equilibrium coefficient
k_B = Boltzmann constant, J K^{-1}
MW = molar mass, kg mol^{-1}
n = number of observations
n_e = number of single events
NNN = next-nearest-neighbors
p = number of parameters to be estimated
p_i = partial pressure of species i, Pa
p_t = total pressure, Pa
PA = proton affinity, J mol^{-1}
r = elementary reaction rate, mol $kg_{cat}^{-1}\ s^{-1}$
R = universal gas constant, J $mol^{-1}\ K^{-1}$
R_i = net rate of formation of species i, mol $kg_{cat}^{-1}\ s^{-1}$
S = objective function
S_{BET} = BET surface area, $m^2\ g^{-1}$
t = time, s
T = temperature, K
T_m = mean temperature, K
v = number of responses per observation
$\hat{V}$ = estimated covariance matrix
V_{micro} = micropore volume, $cm^3\ g^{-1}$
w = weighting factor
W = catalyst mass, kg_{cat}

Greek symbols

β = β-scission
ΔH_+ = catalyst dependent parameter accounting for acid strength, J mol^{-1}
$\Delta H^{0,\ddagger}$ = single-event standard activation enthalpy, J mol^{-1}
ΔH^0_{pr} = standard protonation enthalpy, J mol^{-1}
ΔH^0_{stab} = standard stabilization enthalpy, J mol^{-1}
$\Delta S^{0,\ddagger}$ = single-event standard activation entropy, J $mol^{-1}\ K^{-1}$
ρ = binary correlation coefficient
σ = symmetry number
τ = mean residence time in the reactor, s^{-1}

Superscripts

$\ddagger$ = transition state
0 = initial, feed, standard
reac = reactant

Subscripts

alk = alkylation
app = apparent
dep = deprotonation
gas = gas phase
gl = global
htf = hydride transfer
*i*C8 = 2,2,4-trimethylpentane
iso = isomerization
pcp = PCP (protonated cyclopropane) isomerization
pr = protonation
proto = protolytic scission
zeo = zeolite

Literature Cited

1. Degnan TF Jr. Applications of zeolites in petroleum refining. *Top Catal*. 2000;13(4):349–356.
2. Stöcker M. Gas phase catalysis by zeolites. *Micropor Mesopor Mater*. 2005;82(3):257–292.
3. Vermeiren W, Gilson J-P. Impact of zeolites on the petroleum and petrochemical industry. *Top Catal*. 2009;52(9):1131–1161.
4. Kung HH, Williams BA, Babitz SM, Miller JT, Snurr RQ. Towards understanding the enhanced cracking activity of steamed Y zeolites. *Catal Today*. 1999;52(1):91–98.
5. Bhering DL, Ramírez-Solís A, Mota CJA. A density functional theory based approach to extraframework aluminum species. *J Phys Chem B*. 2003;107(18):4342–4347.
6. Pine LA, Maher PJ, Wachter WA. Prediction of cracking catalyst behavior by a zeolite unit-cell size model. *J Catal*. 1984;85(2):466–476.
7. Hunger M. *Catalytically active sites: generation and characterization*. In: Cejka J, Corma A, Zones S, editors. *Zeolites and Catalysis, Synthesis, Reactions and Applications*, Vol. 2. Weinheim: Wiley-VCH Verlag GmbH & Co., 2010:493–546.
8. Narbeshuber TF, Brait A, Seshan K, Lercher JA. The influence of extraframework aluminum on H-FAU catalyzed cracking of light alkenes. *Appl Catal A*. 1996;146(1):119–129.
9. Xu B, Bordiga S, Prins R, van Bokhoven JA. Effect of framework Si/Al ratio and extra-framework aluminum on the catalytic activity of Y zeolite. *Appl Catal A*. 2007;333(2):245–253.
10. Babitz SM, Williams BA, Miller JT, Snurr RQ, Haag WO, Kung HH. Monomolecular cracking of *n*-hexane on Y, MOR, and ZSM-5 zeolites. *Appl Catal A*. 1999;179(1–2):71–86.
11. van Bokhoven JA, Williams BA, Ji W, Koningsberger DC, Kung HH, Miller JT. Observation of a compensation relation for monomolecular alkane cracking by zeolites: the dominant role of reactant sorption. *J Catal*. 2004;224(1):50–59.
12. Ramachandran CE, Williams BA, van Bokhoven JA, Miller JT. Observation of a compensation relation for *n*-hexane adsorption in zeolites with different structures: implications for catalytic activity. *J Catal*. 2005;233(1):100–108.
13. Katada N, Suzuki K, Noda T, Miyatani W, Taniguchi F, Niwa M. Correlation of the cracking activity with solid acidity and adsorption property on zeolites. *Appl Catal A*. 2010;373(1–2):208–213.
14. Kotrel S, Rosynek MP, Lunsford JH. Intrinsic catalytic cracking activity of hexane over H–ZSM-5, H–BEA and H–Y zeolites. *J Phys Chem B*. 1999;103(5):818–824.
15. Bhan A, Gounder R, Macht J, Iglesia E. Entropy considerations in monomolecular cracking of alkanes on acidic zeolites. *J Catal*. 2008;253(1):221–224.
16. De Moor BA, Reyniers M-F, Gobin OC, Lercher JA, Marin GB. Adsorption of C2–C8 *n*-alkanes in zeolites. *J Phys Chem C*. 2010;115(4):1204–1219.
17. Gounder R, Iglesia E. Catalytic consequences of spatial constraints and acid site location for monomolecular alkane activation on zeolites. *J Am Chem Soc*. 2009;131(5):1958–1971.
18. Gounder R, Iglesia E. Effect of partial confinement on the specificity of monomolecular alkane reactions for acid sites in side pockets of mordenite. *Angew Chem Int Ed*. 2010;49(4):808–811.
19. Costa C, Lopes JM, Lemos F, Ramôa Ribeiro F. Activity–acidity relationship in zeolite Y. Part 3. Application of Brönsted type equations. *J Mol Catal A: Chem*. 1999;144(1):233–238.
20. Costa C, Dzikh IP, Lopes JM, Lemos F, Ramôa Ribeiro F. Activity–acidity relationship in zeolite ZSM-5. Application of Brönsted-type equations. *J Mol Catal A: Chem*. 2000;154(1–2):193–201.
21. Lemos F, Lemos MANDA, Wang X, Ramos Pinto R, Borges P, Costa C, Ramôa Ribeiro F. *Analysis and modelling of multi-site acid catalysts*. In: Derouane EG, Parmon V, Lemos F, Ramôa Ribeiro F, editors. *Principles and Methods for Accelerated Catalyst Design and Testing*. Dordrecht: Kluwer Academic Publishers, 2002:217–243.
22. Borges P, Ramos Pinto R, Lemos MANDA, Lemos F, Védrine JC, Derouane EG, Ramóa Ribeiro F. Activity–acidity relationship for alkane cracking over zeolites: *n*-hexane cracking over HZSM-5. *J Mol Catal A: Chem*. 2005;229(1–2):127–135.
23. Borges P, Ramos Pinto R, Oliveira P, Lemos MANDA, Lemos F, Védrine JC, Derouane EG, Ramôa Ribeiro F. Contributions for the study of the acid transformation of hydrocarbons over zeolites. *J Mol Catal A: Chem*. 2009;305(1–2):60–68.
24. Fonseca N, Lemos F, Laforge S, Magnoux P, Ramôa Ribeiro F. Influence of acidity on the H-Y zeolite performance in *n*-decane catalytic cracking: evidence of a series/parallel mechanism. *Reac Kinet Mech Catal*. 2010;100(2):249–263.
25. Oliveira P, Borges P, Ramos Pinto R, Lemos MANDA, Lemos F, Védrine JC, Ramôa Ribeiro F. Light olefin transformation over ZSM-5 zeolites with different acid strengths—A kinetic model. *Appl Catal A*. 2010;384(1–2):177–185.
26. Dumesic JA, Rudd DF, Aparicio LM, Rekoske JE, Treviño AA. *The Microkinetics of Heterogeneous Catalysis*. Washington, DC: American Chemical Society, 1993.
27. Yaluris G, Madon RJ, Rudd DF, Dumesic JA. Catalytic cycles and selectivity of hydrocarbon cracking on Y-zeolite-based catalysts. *Ind Eng Chem Res*. 1994;33(12):2913–2923.
28. Yaluris G, Rekoske JE, Aparicio LM, Madon RJ, Dumesic JA. Isobutane cracking over Y-zeolites. I. Development of a kinetic model. *J Catal*. 1995;153(1):54–64.

29. Yaluris G, Madon RJ, Dumesic JA. Catalytic ramifications of steam deactivation of Y zeolites: an analysis using 2-methylhexane cracking. *J Catal*. 1999;186(1):134–146.
30. Watson BA, Klein MT, Harding RH. Mechanistic modeling of *n*-heptane cracking on HZSM-5. *Ind Eng Chem Res*. 1996;35(5):1506–1516.
31. Watson BA, Klein MT, Harding RH. Catalytic cracking of alkylbenzenes: modeling the reaction pathways and mechanisms. *Appl Catal A*. 1997;160(1):13–39.
32. Watson BA, Klein MT, Harding RH. Mechanistic modeling of a 1-phenyloctane/*n*-hexadecane mixture on rare earth Y zeolite. *Ind Eng Chem Res*. 1997;36(8):2954–2963.
33. Martens GG, Marin GB, Martens JA, Jacobs PA, Baron GV. A fundamental kinetic model for hydrocracking of C_8 to C_{12} alkanes on Pt/US–Y zeolites. *J Catal*. 2000;195(2):253–267.
34. Thybaut JW, Marin GB, Baron GV, Jacobs PA, Martens JA. Alkene protonation enthalpy determination from fundamental kinetic modeling of alkane hydroconversion on Pt/H-(US)Y-zeolite. *J Catal*. 2001;202(2):324–339.
35. Dewachtere NV, Santaella F, Froment GF. Application of a single-event kinetic model in the simulation of an industrial riser reactor for the catalytic cracking of vacuum gas oil. *Chem Eng Sci*. 1999;54(15–16):3653–3660.
36. Beirnaert HC, Alleman JR, Marin GB. A fundamental kinetic model for the catalytic cracking of alkanes on a USY zeolite in the presence of coke formation. *Ind Eng Chem Res*. 2001;40(5):1337–1347.
37. Quintana-Solórzano R, Thybaut JW, Marin GB. A single-event microkinetic analysis of the catalytic cracking of (cyclo)alkanes on an equilibrium catalyst in the absence of coke formation. *Chem Eng Sci*. 2007;62(18–20):5033–5038.
38. Van Borm R, Aerts A, Reyniers M-F, Martens JA, Marin GB. Catalytic cracking of 2,2,4-trimethylpentane on FAU, MFI, and bimodal porous materials: influence of acid properties and pore topology. *Ind Eng Chem Res*. 2010;49(15):6915–6823.
39. Quintana-Solórzano R, Thybaut JW, Marin GB, Lødeng R, Holmen A. Single-event microkinetics for coke formation in catalytic cracking. *Catal Today*. 2005;107–108:619–629.
40. Bezman RD. Chemical stability of hydrothermally dealuminated Y-type zeolites: a catalyst manufacturer and user's perspective. *Stud Surf Sci Catal*. 1991;68:305–313.
41. Remy MJ, Stanica D, Poncelet G, Feijen EJP, Grobet PJ, Martens JA, Jacobs PA. Dealuminated H-Y zeolites: relation between physicochemical properties and catalytic activity in heptane and decane isomerization. *J Phys Chem*. 1996;100(30):12440–12447.
42. Boréave A, Auroux A, Guimon C. Nature and strength of acid sites in HY zeolites: a multitechnical approach. *Micropor Mater*. 1997;11(5–6):275–291.
43. Collignon F, Mariani M, Moreno S, Remy M. Gas phase synthesis of MTBE from methanol and isobutene over dealuminated zeolites. *J Catal*. 1997;166(1):53–66.
44. Morin S, Ayrault P, Gnep NS, Guisnet M. Influence of the framework composition of commercial HFAU zeolites on their activity and selectivity in *m*-xylene transformation. *Appl Catal A*. 1998;166(2):281–292.
45. Reyniers M-F, Tang Y, Marin GB. Influence of coke formation on the conversion of hydrocarbons. II. *i*-Butene on HY-zeolites. *Appl Catal A*. 2000;202(1):65–80.
46. Imbert FE, Gnep NS, Ayrault P, Guisnet M. Effects of commercial HFAU structural parameters over *m*-cresol transformation. *Appl Catal A*. 2001;215(1–2):225–234.
47. Niwa M, Katada N, Sawa M, Murakami Y. Temperature-programmed desorption of ammonia with readsorption based on the derived theoretical equation. *J Phys Chem*. 1995;99(21):8812–8816.
48. Boggs PT, Byrd RH, Rogers JE, Schnabel RB. *User's Reference Guide for ODRPACK Version 2.01 Software for Weighted Orthogonal Distance Regression*. Gaithersburg: National Institute of Standards and Technology, 1992.
49. Petzold LR. Automatic selection of methods for solving stiff and nonstiff systems of ordinary differential equations. *SIAM J Sci Stat Comput*. 1983;4(1):136–148.
50. Rosenbach N Jr, dos Santos APA, Franco M, Mota CJA. The *tert*-butyl cation on zeolite Y: a theoretical and experimental study. *Chem Phys Lett*. 2010;485(1–3):124–128.
51. Boronat M, Corma A. Are carbenium and carbonium ions reactions intermediates in zeolite-catalyzed reactions? *Appl Catal A*. 2008; 336(1–2):2–10.
52. Corma A, Orchillés AV. Current views on the mechanism of catalytic cracking. *Micropor Mesopor Mater*. 2000;35–36:21–30.
53. Rigby AM, Kramer GJ, van Santen RA. Mechanisms of hydrocarbon conversion in zeolites: a quantum mechanical study. *J Catal*. 1997;170(1):1–10.
54. Tuma C, Sauer J. Protonated isobutene in zeolites: *tert*-butyl cation or alkoxide? *Angew Chem Int Ed*. 2005;44(30):4769–4771.
55. Haw JF. Zeolite acid strength and reaction mechanisms in catalysis. *Phys Chem Chem Phys*. 2002;4(22):5431–5441.
56. Kazansky VB. Adsorbed carbocations as transition states in heterogeneous acid catalyzed transformations of hydrocarbons. *Catal Today*. 1999;51(3–4):419–434.
57. Baltanas MA, Van Raemdonck KK, Froment GF, Mohedas SR. Fundamental kinetic modeling of hydroisomerization and hydrocracking on noble-metal-loaded faujasites. 1. Rate parameters for hydroisomerization. *Ind Eng Chem Res*. 1989;28:899–910.
58. Baltanas MA, Froment GF. Computer generation of reaction networks and calculation of product distributions in the hydroisomerization and hydrocracking of paraffins on Pt-containing bifunctional catalysts. *Comp Chem Eng*. 1985;9:71–81.
59. Feng W, Vynckier E, Froment GF. Single-event kinetics of catalytic cracking. *Ind Eng Chem Res*. 1993;32(12):2997–3005.
60. Martens GG, Thybaut JW, Marin GB. Single-event rate parameters for the hydrocracking of cycloalkanes on Pt/US-Y zeolites. *AIChE J*. 2001;47(7):1607–1622.
61. Willems PA, Froment GF. Kinetic modeling of the thermal cracking of hydrocarbons. 1. Calculation of frequency factors. *Ind Eng Chem Res*. 1988;27:1959–1966.
62. Sanchez-Castillo MA, Agarwal N, Miller C, Cortright RD, Madon RJ, Dumesic JA. Reaction kinetics study and analysis of reaction schemes for isobutane conversion over USY zeolite. *J Catal*. 2002;205(1):67–85.
63. Thybaut JW, Laxmi Narasimhan CS, Marin GB, Denayer JFM, Baron GV, Jacobs PA, Martens JA. Alkylcarbenium ion concentrations in zeolite pores during octane hydrocracking on Pt/H-USY zeolite. *Catal Letters*. 2004;94(1–2):81–88.
64. Corma A, Miguel PJ, Orchillés AV. The role of reaction temperature and cracking catalyst characteristics in determining the relative rates of protolytic cracking, chain propagation, and hydrogen transfer. *J Catal*. 1994;145(1):171–180.
65. Brouwer DM. PMR spectroscopic investigation of structures, stabilities, and rearrangement recations of C_4–C_7 tertiary carbonium ions in HF–SbF_5. *Recl Trav Chim Pay-Bas*. 1968;87(3):210–224.
66. Saunders M, Hagen EL. Rapid rearrangements in the *t*-amyl cation and the relative sign of the coupling constants. *J Am Chem Soc*. 1968;90(9):2436–2437.
67. Brouwer DM. *Reactions of alkylcarbenium ions in relation to isomerization and cracking of hydrocarbons*. In: Prins R, Schuit GCA, editors. *Chemistry and Chemical Engineering of Catalytic Processes*. Alphen a/d Rijn: Sijthoff & Noordhoff, 1980:137–160.
68. Natal-Santiago MA, Alcalá R, Dumesic JA. DFT study of the isomerization of hexyl species involved in the acid-catalyzed conversion of 2-methyl-pentene-2. *J Catal*. 1999;181(1):124–144.
69. Kramer GM, McVicker GB, Ziemiak JJ. On the question of carbonium ions as intermediates over silica–alumina and acidic zeolites. *J Catal*. 1985;92(2):355–363.
70. Craciun I, Reyniers M-F, Marin GB. Effects of acid properties of Y zeolites on the liquid-phase alkylation of benzene with 1-octene: a reaction path analysis. *J Mol Catal A: Chem*. 2007;277(1–2):1–14.

Manuscript received Jan. 24, 2012, and final revision received Apr. 24, 2012.